Control of Ultracold Photodissociation with Magnetic Fields

M. McDonald,[1,†] I. Majewska,[2] C.-H. Lee,[1] S. S. Kondov,[1] B. H. McGuyer,[1,‡] R. Moszynski,[2] and T. Zelevinsky[1,*]

[1]*Department of Physics, Columbia University, 538 West 120th Street, New York, New York 10027-5255, USA*
[2]*Quantum Chemistry Laboratory, Department of Chemistry, University of Warsaw, Pasteura 1, 02-093 Warsaw, Poland*

Photodissociation of a molecule produces a spatial distribution of photofragments determined by the molecular structure and the characteristics of the dissociating light. Performing this basic reaction at ultracold temperatures allows its quantum mechanical features to dominate. In this regime, weak applied fields can be used to control the reaction. Here, we photodissociate ultracold diatomic strontium in magnetic fields below 10 G and observe striking changes in photofragment angular distributions. The observations are in excellent agreement with a multichannel quantum chemistry model that includes nonadiabatic effects and predicts strong mixing of partial waves in the photofragment energy continuum. The experiment is enabled by precise quantum-state control of the molecules.

Chemical reactions at cold and ultracold temperatures exhibit quantum mechanical behavior, since at these low kinetic energies reactions possess a strong sensitivity to the details of intermolecular interactions. Moreover, when the reactants are prepared at ultracold temperatures, their internal quantum states can be well controlled, leading to a much greater understanding of the reaction and potentially enabling a complete theoretical description. When a reaction proceeds at such low temperatures, it becomes possible to control its outcome by applying modest electric or magnetic fields. This occurs because the size of Stark or Zeeman shifts can be much greater than the kinetic energy [1,2], and the density of molecular states is high near the threshold, facilitating mixing by external fields [3]. Field control, including coherent control, of collisions and reactions has been investigated theoretically and experimentally for many molecular systems [4–10].

Photodissociation of a diatomic molecule is a basic chemical process where a bond breaks under the influence of light. It is related to photoassociation of an atom pair [11] by time reversal, but has advantages for studies of ultracold chemistry. In photodissociation, thermal averaging of the atomic collision energies is avoided and the internal and motional states of the initial molecules can be precisely engineered, leading to fully quantum-state-controlled reactions and strictly nonclassical phenomena such as matter-wave interference of the reaction products, as initially shown in Ref. [12] in the absence of external fields. Here, we photodissociate ultracold diatomic strontium molecules, $^{88}Sr_2$, and induce dramatic changes in reaction outcomes by applying magnetic fields. The study of photodissociation in the ultracold regime and in the presence of external fields requires us to explicitly include field-induced angular-momentum mixing into the theoretical treatment of this process. While the theory of photodissociation has been extensively developed [13–16] including the effects of magnetic fields [17], previously the total angular momentum was considered a conserved quantum number. In the regime explored here, this is no longer the case. Combined with a multichannel quantum-chemistry molecular model [18,19], the theoretical treatment we have developed here faithfully reproduces all our experimental observations.

In the experiment we directly observe and record the photofragment angular distributions (PADs) in the millikelvin energy regime. The molecules are prepared at microkelvin temperatures in an optical lattice, and are subsequently fragmented with laser light [12]. The one-dimensional lattice is a standing wave of far-off-resonant light at 910 nm and is approximately 1 MHz (or 50 μK) deep. The geometry of the setup is defined in Fig. 1(a). Photodissociation results in two counterpropagating photofragments, an atom in the ground state $^1S_0$, and an atom in the electronically excited state $^3P_1$ which decays to $^1S_0$ with a 22 μs lifetime. These atoms are absorption imaged using a charge-coupled device camera on the strong Sr transition at 461 nm. The imaging light is turned on for a short duration of $\sim$10 μs, at a time τ (between 250 and 600 μs) after the 20–50 μs photodissociation pulse at 689 nm. During this time τ, the photofragments freely expand and effectively form spherical shells with radii determined by the frequency of the photodissociation light and the Zeeman shifts of the atomic continua. The camera is nearly on axis with the lattice, thus capturing a two-dimensional projection of the spherical shells since the atoms effectively originate from a point source. The laboratory quantum axis points along the applied magnetic field $\vec{B}$, which has a vertical orientation that defines the polar angle θ and azimuthal angle ϕ. The dependence of the photofragment density on these angles is our key observable and encodes
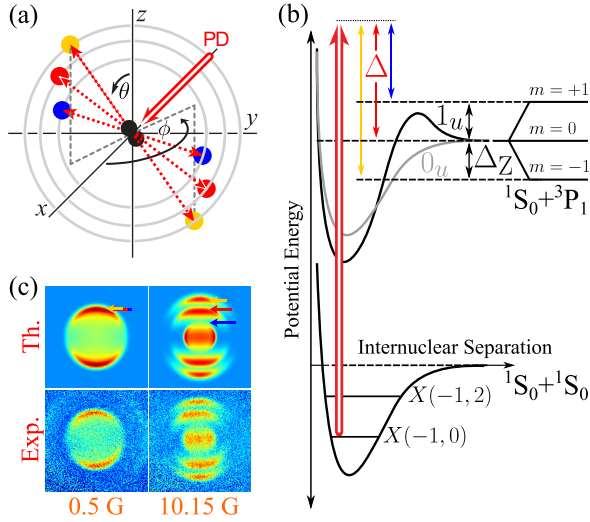
FIG. 1. (a) Geometry of the photodissociation process. The molecules are trapped in an optical lattice at the origin, while the photodissociation (PD) laser propagates along the x axis. The polar angle θ and azimuthal angle ϕ are defined as shown to describe the photofragment angular distributions (PADs). The radii of the spherical shells containing the fragments after a fixed expansion time are given by the frequency of the PD laser and the Zeeman shifts of different atomic continua. The largest shell corresponds to a negative shift (yellow), the medium shell to an absence of shift (red), and the smallest shell to a positive shift (blue). A camera points in the $-x$ direction and images a two-dimensional projection of the nested shells. (b) Molecular potentials and quantum states relevant to the experiment. The photodissociation process is designated by the double arrow. The detuning of the PD light from the $m = 0$ Zeeman component of the continuum is Δ, and the symmetric Zeeman splitting has a magnitude Δ_Z. The barrier of the 1_u potential has a height of ~ 30 MHz. The numbers in parentheses are v and J_i. (c) An example of calculated and measured PAD images for a process where a small applied magnetic field drastically alters the outcome of the reaction. The two pairs of images differ only by the magnitude of the applied field: $B = 0.5$ G on the left and 10.15 G on the right.

the quantum mechanics of the reaction. The photodissociation light polarization is set to be either vertical or horizontal.

Figure 1(b) illustrates the Sr_2 molecular structure relevant to this work. The molecules are created from ultracold atoms via photoassociation [20] in the least-bound vibrational level, denoted by $v = -1$, of the electronic ground state $X^1\Sigma_g^+$ (correlating to the $^1S_0 + {}^1S_0$ atomic threshold). Initially, the molecules occupy two rotational states with the total angular-momentum quantum numbers $J_i = 0$ and 2, but the $J_i = 2$ population is mostly removed prior to fragmentation by a laser pulse resonant with an excited molecular state. The $J_i = 0$ molecules (with a projection quantum number $M_i = 0$) are coupled by the photodissociation laser to the singly excited continuum above the 0_u and 1_u *ungerade* potentials (correlating to the

$^1S_0 + {}^3P_1$ atomic threshold), where the numbers refer to the total atomic angular momentum projections onto the molecular axis. Under an applied field $B > 0$, the atomic energy levels split by the Zeeman interaction into the $m = -1$, 0, and 1 sublevels, where the energy separation between the neighboring sublevels is $h\Delta_Z = 1.5\mu_B B$ and μ_B is the Bohr magneton. The radius of each photofragment shell is $v\tau$ where $v = \sqrt{h(\Delta - m\Delta_Z)/m_{Sr}}$ is the velocity, h is the Planck constant, Δ is the frequency detuning of the photodissociation light from the $m = 0$ component of the continuum, and m_{Sr} is the atomic mass of Sr.

If the photodissociation laser detuning is large and negative, $\Delta < -\Delta_Z$, no photofragments should be detectable because the target energy is below the lowest threshold. If the detuning is small and negative, $-\Delta_Z < \Delta < 0$, then only one fragment shell should be visible, corresponding to $m = -1$. If the detuning is small and positive, $0 < \Delta < \Delta_Z$, we expect to observe two fragment shells, with $m = -1$ and 0. Finally, if the detuning is large and positive, $\Delta_Z < \Delta$, we expect three fragment shells with all possible values of m. This is the case in the example of Fig. 1(c) that shows a strong alteration of the PAD for $B = 10.15$ G compared to 0.5 G.

Here we make the distinction between the angular-momentum projection quantum numbers m and M, the latter denoting the projection of the total angular momentum J in the continuum. Electric-dipole ($E1$) selection rules require $M = M_i = 0$ if the photodissociation laser polarization is parallel to the quantum axis and $M = \pm 1$ if the polarization is perpendicular. In contrast, there are no such selection rules for the atomic magnetic sublevels m which can be superpositions of several M. A thorough treatment is included in the Supplemental Material [21].

When a $J_i = 0$ diatomic molecule is photodissociated via a one-photon $E1$ process without an applied field, we expect and observe a dipolar-shaped PAD with an axis set by the laser polarization [12], as in the nearly field-free case of Fig. 1(c). This can be understood either by visualizing a spherically symmetric molecule absorbing light with a dipolar probability distribution, or by applying angular-momentum selection rules that require $J = 1$ for the outgoing channel, which has a dipolar angular distribution with a single spatial node. We find that with a nonzero B this is no longer the case, and instead observe complicated structures with multiple nodes.

The main results of the experiment and theory are summarized in Fig. 2. The two-dimensional projections of the PADs onto the imaging plane, with the detuning $\Delta = 29.2$ MHz, are shown in Fig. 2(a) for a progression of magnetic fields B from 0.5 to 10.15 G. The removal of the $J_i = 2$ molecules is imperfect which results in the very faint outermost shell that can be ignored. The top pair of rows corresponds to parallel light polarization and the bottom pair to perpendicular polarization. We observe a transformation from simple dipolar patterns at $B = 0$ to more
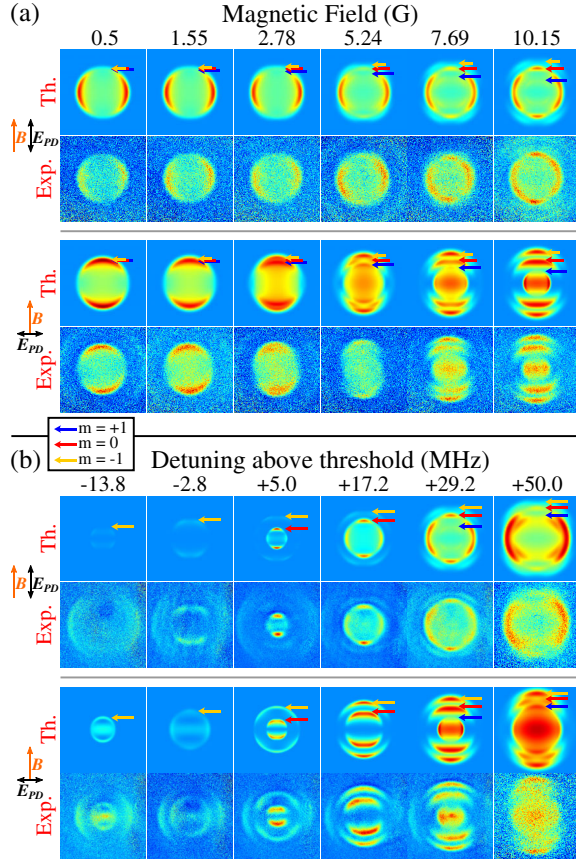
FIG. 2. Tuning of the photodissociation reaction with small magnetic fields, across a range of energies. The color coding for the continuum Zeeman components is consistent between Figs. 1 and 2. (a) Theoretical and experimental images of PADs as the magnetic field B is increased from 0.5 to 10.15 G, for the detuning $\Delta = 29.2$ MHz. (b) Theoretical and experimental PAD images at $B = 10.15$ G, covering a range of Δ from -13.8 to 50.0 MHz. As indicated in Fig. 1, additional channels ($m = -1$, 0, and 1) become available in the continuum as Δ increases, leading to extra photofragment shells. In some of the experimental images, the faint outermost shell is the result of incidental photodissociation of residual $J = 2$ molecules and can be ignored. The top and bottom pairs of rows in both (a) and (b) correspond to the light polarization parallel and perpendicular to $\vec{B}$, respectively. Typically, 300 experiments with atoms and 300 without atoms (for background subtraction) are averaged to obtain each experimental PAD image. The experimental images use an arbitrary brightness scale, and the relative transition strengths for different images can be inferred from this data only qualitatively. Within each PAD, however, relative transition strengths to different m's are more accurately reflected in the relative brightness of the rings.

complex patterns that exhibit a multiple-node structure at 10.15 G. Figure 2(b) shows PADs that are observed when B is kept fixed at 10.15 G while Δ is varied from -13.8 to 50.0 MHz, again for both cases of linear light polarization. For the entire range of continuum energies, we observe PADs that exhibit a multinode structure. As Δ and B are

varied, the angular dependence, or anisotropy, of the outgoing PAD is strongly affected. The zero-field evolution of the PADs with energy for this continuum is discussed in Ref. [12]. All additional features observed here are due to the continuum partial waves J being strongly mixed by the applied field.

As Fig. 2 demonstrates, our theoretical results are in excellent agreement with the experimental data. The theory involves extending the standard treatment of diatomic photodissociation to the case of mixed angular momenta in the presence of a magnetic field, and applying it to the quantum-chemistry model of the $^{88}Sr_2$ molecule [18,19]. As detailed in Ref. [21], the PADs can be described by the expansion

$$I(\theta, \phi) \propto \beta_0 \left(1 + \sum_{\mu=1}^{\infty} \sum_{\nu=0}^{\mu} \beta_{\mu\nu} P_\mu^\nu(\cos\theta) \cos(\nu\phi) \right) \quad (1)$$

where $P_\mu^\nu(\cos\theta)$ are the associated Legendre polynomials and the $\beta_{\mu\nu}$ coefficients are called anisotropy parameters. In the case of parallel light polarization, the PADs are cylindrically symmetric (no ϕ dependence) [12], and we set $\beta_\mu \equiv \beta_{\mu 0}$ while all other $\beta_{\mu\nu}$ vanish. The μ are even for homonuclear dimers. The anisotropy parameters in Eq. (1) can be evaluated from Fermi's golden rule after properly representing the initial (bound-state) and final (continuum) wave functions, including mixing of the angular momenta J_i and J by the magnetic field.

The most salient feature of ultracold photodissociation in nonzero magnetic fields is the dramatic change of the PADs which tend to become significantly more complex as the field is increased. Figures 3(a) and 3(b) compare the photodissociation outcome at $B = 10.15$ G [also in the top right of Fig. 2(a)] to that at $B = 0$. Besides the appearance of an outer shell caused by Zeeman splitting in the continuum, the central $m = 0$ shell gains additional lobes. This effect arises from the magnetic field admixing higher partial waves in the continuum, as the density of states is particularly high near the dissociation threshold [3]. We show this directly by simulating the image of the PAD on the right panel of Fig. 3(a) while using a series of cutoff partial waves J_{max} that are included in the continuum wave function. The result is in Fig. 3(c). The PAD evolves with increasing J_{max}, only reproducing the data at $J_{max} = 5$. We have confirmed that increasing J_{max} further does not alter the PAD appreciably. ($J_{max} = 1$ if $B = 0$.) The evolution of the PADs with increasing magnetic field can be alternatively described by plotting the anisotropy parameters β_μ as functions of B. Figures 3(d)–3(h) show this for the PAD in Fig. 3(a), for anisotropies of order $\mu = 0$ through 8 that we can resolve in the experiment. The curves correspond to contributions from pure and mixed exit-channel partial waves of Eq. (10) in Ref. [21], with J_k, J_k' varying from 1 to 5. These plots directly show that higher-order anisotropy ($\mu > 4$) arises already at ~ 1 G and is dominated by the
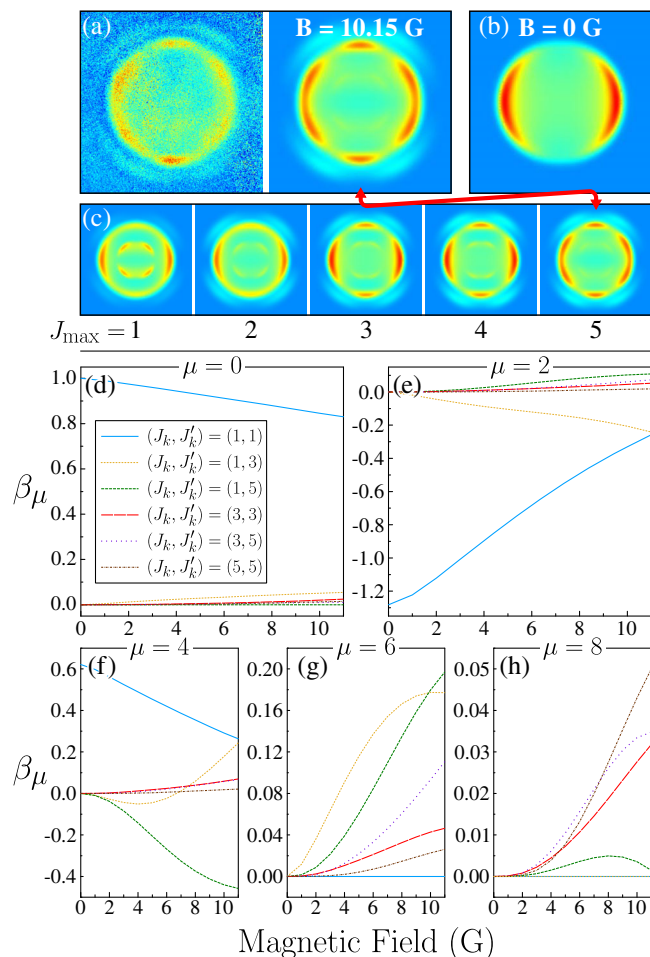
FIG. 3. Mixing of the continuum partial waves with a small magnetic field. (a) Experimental and calculated PAD images for photodissociation at $B = 10.15$ G. The laser polarization is parallel to $\vec{B}$ and the detuning is $\Delta = 29.2$ MHz. The brightest fragment shell here corresponds to $m = 0$. (b) For comparison, a calculated PAD for $B = 0$ consists of a simple dipolar pattern corresponding to $J = 1$. The quantum numbers $m = -1, 0, 1$ are unresolved. (c) Calculated PADs of the process in (a), each image including contributions only up to the maximum partial wave $J_{max} = 1$ through 5 that is included in the multichannel continuum wave function, as labeled. Agreement with experiment is reached for $J_{max} = 5$. (d)–(h) Plots of the anisotropy parameters β_μ versus the field strength B for the dominant $m = 0$ component of the PAD in (a). The contributions of individual continuum angular-momentum pairs (J, J') are shown (with $J_{max} = 5$), where the indexed notation corresponds to that of Eq. (10) in Ref. [21]. The curves in (d) are also normalized by the total β_0 and illustrate the relative contributions of the partial wave pairs to the photodissociation transition strength [21].

admixing of increasingly higher angular momenta in the continuum. Note in the plots of Figs. 3(d)–3(h) that if $B = 0$, the maximum anisotropy order is $\mu = 4$ for our quantum numbers.

We have shown that the reaction of photodissociation can be strongly altered in the ultracold regime by small

applied magnetic fields. In this work, the fragmentation of $^{88}Sr_2$ molecules was explored for a range of fields from 0 to 10 G, and for a variety of energies above threshold in the 0–2 mK range. The near-threshold continuum has a high density of partial waves that are readily mixed by the field, resulting in pronounced changes of the photofragment angular distributions. The theory of photodissociation, after explicit accounting for field-induced mixing of angular momenta in the bound and continuum states, and combined with an accurate quantum-chemistry molecular model, has yielded excellent agreement with experimental data. The experiment and its clear interpretation was made possible by preparing the molecules in well-defined quantum states. We have shown that ultracold molecule techniques allow a high level of control over basic chemical reactions with weak applied fields. Moreover, this work serves as a test of *ab initio* molecular theory in the continuum.

*tanya.zelevinsky@columbia.edu
†Present address: Department of Physics, University of Chicago, 929 East 57th Street GCIS ESB11, Chicago, IL 60637, USA.
‡Present address: Facebook, Inc., 1 Hacker Way, Menlo Park, CA 94025, USA.

[1] N. Balakrishnan, Perspective: Ultracold molecules and the dawn of cold controlled chemistry, J. Chem. Phys. 145, 150901 (2016).

[2] M. Lemeshko, R. V. Krems, J. M. Doyle, and S. Kais, Manipulation of molecules with electromagnetic fields, Mol. Phys. 111, 1648 (2013).

[3] B. H. McGuyer, M. McDonald, G. Z. Iwata, W. Skomorowski, R. Moszynski, and T. Zelevinsky, Control of Optical Transitions with Magnetic Fields in Weakly Bound Molecules, Phys. Rev. Lett. 115, 053001 (2015).

[4] K.-K. Ni, S. Ospelkaus, D. Wang, G. Quéméner, B. Neyenhuis, M. H. G. de Miranda, J. L. Bohn, J. Ye, and D. S. Jin, Dipolar collisions of polar molecules in the quantum regime, Nature (London) 464, 1324 (2010).

[5] M. H. G. de Miranda, A. Chotia, B. Neyenhuis, D. Wang, G. Quéméner, S. Ospelkaus, J. L. Bohn, J. Ye, and D. S. Jin, Controlling the quantum stereodynamics of ultracold bimolecular reactions, Nat. Phys. 7, 502 (2011).

[6] G. Quéméner and J. L. Bohn, Ultracold molecular collisions in combined electric and magnetic fields, Phys. Rev. A 88, 012706 (2013).

[7] L. P. Parazzoli, N. J. Fitch, P. S. Żuchowski, J. M. Hutson, and H. J. Lewandowski, Large Effects of Electric Fields on

Atom-Molecule Collisions at Millikelvin Temperatures, Phys. Rev. Lett. **106**, 193201 (2011).

[8] T. V. Tscherbul and R. V. Krems, Quantum theory of chemical reactions in the presence of electromagnetic fields, J. Chem. Phys. **129**, 034112 (2008).

[9] M. Shapiro, J. W. Hepburn, and P. Brumer, Simplified laser control of unimolecular reactions: Simultaneous (ω_1, ω_3) excitation, Chem. Phys. Lett. **149**, 451 (1988).

[10] B. Sheehy, B. Walker, and L. F. DiMauro, Phase Control in the Two-Color Photodissociation of HD^+, Phys. Rev. Lett. **74**, 4799 (1995).

[11] K. M. Jones, E. Tiesinga, P. D. Lett, and P. S. Julienne, Ultracold photoassociation spectroscopy: Long-range molecules and atomic scattering, Rev. Mod. Phys. **78**, 483 (2006).

[12] M. McDonald, B. H. McGuyer, F. Apfelbeck, C.-H. Lee, I. Majewska, R. Moszynski, and T. Zelevinsky, Photodissociation of ultracold diatomic strontium molecules with quantum state control, Nature (London) **534**, 122 (2016).

[13] R. N. Zare, Photoejection dynamics, Mol. Photochem. **4**, 1 (1972).

[14] G. G. Balint-Kurti and M. Shapiro, Photofragmentation of triatomic molecules. Theory of angular and state distribution of product fragments, Chem. Phys. **61**, 137 (1981).

[15] S. E. Choi and R. B. Bernstein, Theory of oriented symmetric-top molecule beams: Precession, degree of orientation, and photofragmentation of rotationally state-selected molecules, J. Chem. Phys. **85**, 150 (1986).

[16] V. V. Kuznetsov and O. S. Vasyutinskii, Photofragment angular momentum distribution beyond the axial recoil approximation: The role of molecular axis rotation, J. Chem. Phys. **123**, 034307 (2005).

[17] J. A. Beswick, Angular distribution of photo-predissociation fragments in the presence of a mangetic field, Chem. Phys. **42**, 191 (1979).

[18] W. Skomorowski, F. Pawłowski, C. P. Koch, and R. Moszynski, Rovibrational dynamics of the strontium molecule in the $A^1\Sigma_u^+$, $c^3\Pi_u$, and $a^3\Sigma_u^+$ manifold from

state-of-the-art *ab initio* calculations, J. Chem. Phys. **136**, 194306 (2012).

[19] M. Borkowski, P. Morzyński, R. Ciuryło, P. S. Julienne, M. Yan, B. J. DeSalvo, and T. C. Killian, Mass scaling and nonadiabatic effects in photoassociation spectroscopy of ultracold strontium atoms, Phys. Rev. A **90**, 032713 (2014).

[20] G. Reinaudi, C. B. Osborn, M. McDonald, S. Kotochigova, and T. Zelevinsky, Optical Production of Stable Ultracold $^{88}Sr_2$ Molecules, Phys. Rev. Lett. **109**, 115303 (2012).

[21] See Supplemental Material at http://link.aps.org/supplemental/10.1103/PhysRevLett.120.033201 for the quantum mechanical description of photodissociation in applied magnetic fields, which includes Refs. [22–29].

[22] P. S. Shternin and O. S. Vasyutinskii, The parity-adapted basis set in the formulation of the photofragment angular momentum polarization problem: The role of the Coriolis interaction, J. Chem. Phys. **128**, 194314 (2008).

[23] G. G. Balint-Kurti and M. Shapiro, in *Advances in Chemical Physics: Photodissociation and Photoionization*, edited by K. P. Lawley (John Wiley & Sons, Inc., Hoboken, New Jersey, 1985), Vol. 60.

[24] J. G. Underwood and I. Powis, Photodissociation of polarized diatomic molecules in the axial recoil limit: Control of atomic polarization, J. Chem. Phys. **113**, 7119 (2000).

[25] M. Born and K. Huang, *Dynamical Theory of Crystal Lattices* (Oxford University Press, Oxford, 1956).

[26] B. Bussery-Honvault, J.-M. Launay, T. Korona, and R. Moszynski, Theoretical spectroscopy of the calcium dimer in the $A^1\Sigma_u^+$, $c^3\Pi_u$, and $a^3\Sigma_u^+$ manifolds: An *ab initio* nonadiabatic treatment, J. Chem. Phys. **125**, 114315 (2006).

[27] R. D. Levine, *Quantum Mechanics of Molecular Rate Processes* (Oxford University Press, Oxford, 1969).

[28] B. R. Johnson, The multichannel log-derivative method for scattering calculations, J. Comput. Phys. **13**, 445 (1973).

[29] R. V. Krems and A. Dalgarno, Quantum-mechanical theory of atom-molecule and molecular collisions in a magnetic field: Spin depolarization, J. Chem. Phys. **120**, 2296 (2004).